TRANSIENT AND MEAN STRUCTURES IN DRIVEN-CAVITY FLOW

Francisco Aurilo Azevedo Pinho, aurilopinho@uft.edu.br
Universidade Federal do Tocantins

Aristeu Silveira Neto, aristeus@cnpq.gov.br
Universidade Federal de Uberlândia

Abstract. *The purpose of this assignment is to show the large-eddy simulation of driven-cavity flow results. In this simulation a finite volume code was used, which is based on a fourth order central difference schema to spatial advective and to diffusive terms and a second order to pressure terms. A second order, Adams-Bashfort schema, was used for the temporal discretization. Simulations were accomplished to Reynolds number 3200, 10000 and 25000. The first two Reynolds numbers show the main velocity and the fluctuation profile agreeing with experimental and numerical literature results. Like Taylor-Görtler structure was pointed out in all cases and transversal structures flow was found for Reynolds number 10,000.*

Keywords*: driven-cavity; large eddy simulation; dynamic model; Taylor-Görtler*

1. INTRODUÇÃO

The driven cavity flow has attracted the interest of researchers since the mid-twentieth century. This can be proven referring to Burgraff (1966), who is mentioned by several authors as one of the pioneers in studying this problem numerically, and to Pan and Acrivos (1967), who studied numerically and experimentally. In the latter, the authors compare their results with those obtained by Dean and Montagons (1949) and Moffat (1964). Furthermore, in recent works, Sheu and Tsai (2002) has studied numerically the flow in a cubical cavity for Reynolds number 1000, Migeon *et al*. (2003) has performed experiments with the same configuration, and Peng *et al*. (2003) numerically has studied the transition from laminar to chaotic two-dimensional flow, showing that this geometry still attracts great interest.

Some factors have contributed to this interest. The regular geometry and the unambiguously boundary conditions make this problem an ideal case for numerical method testing (Prasad and Koseff, 1989) and (Sheu and Tsai, 2002). This flow provides the opportunity to study the stationary vortex development and a wide range of phenomena that occurs around this, such as secondary vortices, corner vortices and like Taylor-Görtler vortices. Finally, this flow is an idealization of various environmental, geophysics, industrial (Freitas and Street, 1988) and biomedical problems (Migeon *et al*., 2003). A practical applications of the lid driven-cavity flow is the deposition process of liquid films in a surface (Aidum *et al*. 1991). Another application is the flow within the casting cavities used for the microcrystalline material manufacture (Shankar and Deshpande, 2000). This flow is also an idealization of many practical flows, such as "flow over cutouts and repeat slots an the walls of heat exchangers or on the surface of aircraft bodies" (Prasad and Koseff, 1989).

Although the great initial interest in this flow, the details of this topology alone had been disclosed slowly throughout the last the four decades, above all, recent evolutions of experimental techniques, computer developments and the most efficient numerical methodologies were used.

A critical point for the modern engineering development and for the physics of the turbulent flow understanding is the analysis of the temporal evolution and the flow topology. In this direction, the perception of the flow details, the numerical simulations are more efficient than the experimental measurements, for example, the confirmation of the lateral vortices gotten in laboratory by Koseff *et al*. (1983) (Chiang *et al*., 1997). In such a way, the current assignment goal is to analyze the transient structures in lid driven cavity flow in cubical with Reynolds number 3,500, 10,000 and 25.000. Because there are experimental and numerical results with which comparisons can be made for validation of the methods and its implementations, the Reynolds numbers 3,500 and 10,000 were chosen. The Reynolds number 25,000 was chosen by not belonging to the literature yet, and had the existence of the MFLab (Laboratório de Mecânica dos Fluidos) in UFU (Universidade Federal de Uberlândia) that aims at simulation the higher Reynolds numbers.

Beyond the Reynolds number, two other parameters characterize the driven cavity flow problem, the aspect ratio and the spanwise aspect ratio. The aspect ratio (R) is the reason between the height and the length, noticed as $H : L$. The spanwise aspect ratio (SAR) is the reason between width and the length, noticed as $W : L$.

The cubical lid driven-cavity had been studied experimentally by Prasad and Koseff (1989) and numerically by Perng and Street (1989), Deshpande and Milton (1998), Hassan and Barsamian (2001), Sheu and Tsai (2002) and Padillla *et al*. (2005). It is important to highlight the work of Prasad and Koseff (1989) they are boarded numerically and experimentally values of SAR 1:1 and 1:2. This last one studied numerically by Zang *et al*. (1993).

In the lid driven-cavity, Aidum *et al*. (1991) affirm that the flow remains stationary until Reynolds number 1,300,

when the transition occurs for the transient regimen. The laminar flow remains until Reynolds number between 6.000 and 8.000, when the transition to turbulence begins in some cavity regions. With Reynolds number 10,000 the regimen is already completely turbulent.

The works of Sheu and Tsai (2002) and Migeon *et al*. (2003) analyze the low Reynolds numbers stationary flow. The transition process to the transient flow, but still laminar, is studied by Aidum *et al*. (1991) and Chiang *et a*l. (1998). Laminar to turbulent flow transition had been studied by Koseff and Street (1984).

Among the studies of laminar and turbulent flow are distinguished carried through by Prasad and Koseff (1989), Perng and Street (1989) and Deshpande and Milton (1998). The first is an experimental analysis of the flow and the others are numerical analysis of the cases treated in the first one. They had been considered Reynolds number 3,200, to laminar flow, and the 10,000, for the turbulent case.

The turbulence is present in an enormous variety of phenomena. In fluid flow it appears entirely when the governing parameters, as the Reynolds number, becomes enough high to destabilize it. This is basically the natural flow and practical applications. The knowledge of these phenomena can be applied to the industrial equipment projects. As in most effective control of heat exchanges, in improvement of fluid mixture performances, in reduction of drag and the increase of the security of bodies in movement, as they are cars and aircrafts. They can still be used in the analysis of atmospheric phenomena, influencing the way man relates to nature, predicting weather phenomena more effectively, such as droughts, floods and cyclones, as well as, in the good time periods, increasing the possibility of social planning.

Although all these possibilities of uses and advances in turbulent flow modeling, there is still a tool that can solve any flow type, which has extremely complex features in each one of them, either one individually or together. Prodigy is still strongly dependent on a previous flow analysis to obtain a coherent model (Bradshaw, 1997).

The Navier-Stokes equation satisfactorily represents all Newtonian fluid flow phenomena, with not considering the flow type. However numerical solution expectations of all wide ranges of turbulent scales do not exist. Numerical simulations of this type had already been accomplished for moderate values of Reynolds number. These are called Direct Numerical Simulations (DNS). However, as the scale range grows this becomes impracticable, due to the mesh refinement requirement that must cover all scales.

One of the solution proposals for this problem is the use of the Large Eddy Simulation (LES). This methodology, a proposal initially for Smagorinsky (1963), has the goal of dividing the flow scales. The scales that can be captured by the mesh are numerically solved, and the fewer scales whose characteristic mesh size (subgrid scales) are modeled in such a way that the energy that would be wasted by them is wasted in an artificial way by the turbulence model. This model is called subgrid model and one of its characteristics must be simplicity.

The first and most used one of the subgrid models is the Smagorinsky model (Lesieur *et al*., 2005). This model is based on the small scales isotropy, and on the balance hypothesis, according to which the production of turbulent kinetic energy is equally wasted. Later, Germano *et al*. (1991) he considered a model, in which, if he applies a filter in the determined field to get information in the transferring of energy in the intermediate scales between the characteristic size of this filter and the size of the mesh. With this information, the transferring of energy to the subgrid scales is adjusted to the model. By doing so, it assumes that the characteristics of the transference in the two levels are the same ones. This model later was modified by Lilly (1992)

2. MATHEMATICAL MODELS

The current assignment uses primitive variables, three-dimensional equations for incompressible constant property flow to model lid driven-cavity flow. the mass conservation equation and the Navier-Stokes incompressible flow with constant viscosity equations, they result of the application of the Newton's Second Law to Eulerian referential and of Stokes relation for the proportionality enter viscous stress to fluid deformation (White, 2005).

2.1. Filtered Navier-Stokes equations

The Reynolds equations are average of the Navier-Stokes equation. However, a filtered form of the equation is used in the Large-Eddy Simulation. A filter G is defined in such a way that any variable ϕ is given by the addition of filtered component $\bar{\phi}$ and one floating component ϕ^{l},

$$\phi(\vec{x})=\bar{\phi}(\vec{x})+\phi^{l}(\vec{x}) \ . \tag{1}$$

where $\vec{x}$ is the position vector. The filtered component is gotten by the application of this filter to the variable,

$$\bar{\phi}(\vec{x}_o)=\int \phi(\vec{x})G(\vec{x}-\vec{x}_o)\,dx \ . \tag{2}$$

Applying this filter to the mass conservation equation it does not have alter its format. However, in the Navier-Stokes equation a difference due to the not linear term appears,

$$\frac{\partial \overline{u_i}}{\partial t}+\frac{\partial(\overline{u_j}\overline{u_i})}{\partial x_j}=-\frac{1}{\rho}\frac{\partial \overline{p}}{\partial x_i}+\frac{\partial}{\partial x_j}\left(\nu\frac{\partial \overline{u_i}}{\partial x_j}-\tau_{ij}\right)+\overline{\Phi_{ij}}+\overline{f_i}\ . \tag{3}$$

The appearance of the derivative of the subgrid tensor τ_{ij} is noticed:

$$\tau_{ij}=\overline{u_i u_j}-\overline{u_i}\,\overline{u_j}\ . \tag{4}$$

This tensor traditionally is placed next to the diffusive term to call attention to the turbulence in the diffusivity increase, in case of momentum.

2.2. Turbulence models

Boussinesq (1877) proposed the subgrid tensor in the same way that Stokes viscous stressed his model. By doing so, he used the concept of turbulent viscosity in boundary layer on an infinite plain plate. Kolmogorov (1942) considered a generalized form Boussinesq's hypothesis and this has been the form used until current times,

$$\tau_{ij}=-2\nu_t\overline{S}_{ij}+\frac{2}{3}\delta_{ij}\tau_{ij}\ , \tag{5}$$

where ν_t is the turbulent viscosity and S_{ij} is the deformation tensor, it given by:

$$S_{ij}=\frac{1}{2}\left(\frac{\partial u_i}{\partial x_j}+\frac{\partial u_j}{\partial x_i}\right)\ . \tag{6}$$

In such a way it is:

$$\tau_{ij}-\frac{2}{3}\delta_{ij}\tau_{ij}=-\nu_t\left(\frac{\partial u_i}{\partial x_j}+\frac{\partial u_j}{\partial x_i}\right)\ . \tag{7}$$

Note the left side of the equation will count only to the anisotropic part of the subgrid tensor.

2.2.1. Smagorinsky's Model

Smagorinsky, following the idea of the Prandtl's mixture length model (Lesieur *et al*., 2005), considered a subgrid model in which turbulent viscosity is proportional to the mesh characteristic length, and to a characteristic subgrid velocity. The mesh characteristic length is an obvious choice, the characteristic velocity must be related to small scales velocities, it is of velocity variation order on a mesh element. By proportionality constantly adding it, gets to a final expression for turbulent viscosity,

$$\nu_t=(C_s\Delta)^2\sqrt{2\overline{S}_{ij}\overline{S}_{ij}}\ , \tag{8}$$

where C_S is the Smagorinsky's constant.

The Smagorinsky's constant value can be analytically calculated (Lesieur, 1997) and its value is 0,18. This value is a success for isotropic turbulence, as it was expected to be, since isotropy is one of the model assumptions. For non-isotropic flow, as mixing layers, this value must be reduced by the half as suggested by Ferziger (1993). The same author suggests that this reduction may be due to energy inverse cascade. Flowing near the wall in this model fails, because there are large deformations in these regions, therefore high values of turbulent viscosity. However these values must be low, since the turbulence near the wall decreases.

2.2.2. Germano's dynamic model

The dynamic model proposed by Germano *et al*. (1991) and modified for Lilly (1992) suggests the dynamic form of subgrid model adjustment, varying in space and time. An additional filter is used for this, the test filter, with a larger characteristic size than the mesh characteristic size. The model uses the concept of similarity scales, that is, it assumes that the lesser scales captured for the solution and the biggest subgrid scales have similar structures. Thus, the velocity field is filtered and the information is used to calculate turbulent viscosity to be used in the solution.

Using Smagorinsky's model as subgrid model, the model dynamically adjusts the proportionality value between the turbulent viscosity and the deformation tensor module. In this case, the coefficient is given by:

$$C=\frac{1}{2}\frac{L_{ij}M_{ij}}{M_{ij}M_{ij}}, \tag{9}$$

where

$$L_{ij}=\widehat{\overline{u_i}\,\overline{u_j}}-\hat{\overline{u}}_i\hat{\overline{u}}_j . \tag{10}$$

and

$$M_{ij}=\widehat{\Delta^2|\overline{S}|\overline{S}_{ij}}-\Delta^2|\widehat{\overline{S}|\overline{S}_{ij}} . \tag{11}$$

Note the filter test notation with a hat, for example $\hat{\Delta}$ is the test filter characteristic size. The tensors L_{ij} and M_{ij} can explicitly be calculated, since the values in the equations are all known.

Padilla (2004) made a careful study on test filters used for the calculating the dynamic proportionality coefficient. In the current assignment, the weight of the filter used was 0.5 for the filtered variable.

3. NUMERICAL MODEL

For the current assignment a finite volume of computational code for incompressible constant property Navier-Stokes equation solution was developed. A totally explicit second order Adams-Bashforth method was used for both, advective and diffusive terms, a velocity fourth order central differs and pressures according to space discretization. The Germano's dynamics and Smagorinsky subgrid models were also implemented.

3.1. Time discretization

In this assignment the explicit Adams-Bashforth method has been used for both the advective term and for the convective term for the velocity, and fully explicit for the pressure.

$$\frac{(u_i^{n+1}-u_i^n)}{\Delta t}=-\frac{\Delta p^{n+1}}{\Delta x_i}+\frac{3}{2}\left[S(u_i^n)\right]-\frac{1}{2}\left[S(u_i^{n-1})\right], \tag{12}$$

where $S(u)$ is the sum of advective ($A(u)$) diffusive ($D(u)$) terms and the body forces ($F(u)$), and u represents any of the velocity components.

3.2. Pressure-velocity coupling

The pressure-velocity coupling is done by the use of pressure correction method. A velocity field is estimated by considering the pressure field in the previous time, the estimating velocity $\hat{u}_i$ is given by:

$$\hat{u}_i^{n+1}=u_i^n-\Delta t\frac{\Delta p^{n+1}}{\Delta x_i}+\frac{3\Delta t}{2}\left[S(u_i^n)\right]-\frac{\Delta t}{2}\left[S(u_i^{n-1})\right] . \tag{13}$$

The Boundaries condition to estimated velocities are back time velocities.

Subtracting Eq. (13) to Eq. (12), we obtain:

$$u_i^{n+1}-\hat{u}_i^{n+1}=-\Delta t\frac{\Delta(p^{n+1}-p^n)}{\Delta x_i}=-\Delta t\frac{\Delta(p^l)}{\Delta x_i}, \tag{14}$$

where $p^l=p^{n+1}-p^n$ is the pressure correction in time step $n+1$. This equation can be used to velocity correction obtained after the correction of pressure,

$$u_i^{n+1}=\hat{u}_i^{n+1}-\Delta t\frac{\Delta(p^l)}{\Delta x_i} . \tag{15}$$

To obtain a pressure-correction equation, applies the divergent operator to the Eq. (14),

$$-\Delta t\nabla^2(p^l)=\nabla(\vec{u}^{n+1})-\nabla(\hat{\vec{u}}^{n+1}) . \tag{16}$$

where $\nabla^2(p)$ is the pressure curl, $\nabla(\vec{u})$ the velocity divergent and $\nabla(\vec{\tilde{u}})$ the estimated velocity divergent. Since the velocity divergent is null due to incompressible flow mass conservation (Eq. ()),

$$\Delta t \nabla^2(p^l) = \nabla(\hat{\vec{u}}^{n+1}) \,. \tag{17}$$

This equation is solved with null derivative boundaries conditions in all domain face.

3.3. Spatial discretization

Fourth order central difference scheme was used in this assignment for velocity in Eq. (12). In this scheme any variable ϕ and its derivative in e face of control volume are:

$$\phi_e = \frac{7(\phi_P + \phi_E) - (\phi_W + \phi_{EE})}{12} \tag{18}$$

and

$$\left(\frac{\partial \phi}{\partial x_i}\right)_e = \frac{15(\phi_E - \phi_P) - (\phi_{EE} - \phi_w)}{12\,\Delta x_i} \,. \tag{19}$$

respectively.

Transport properties values are evaluated in the volume faces using using means when the value is not available in the face. A second order central difference scheme is used in the cross terms from the Navier-Stokes (Eq. 2), in the pressure correction and in velocity correction equations.

4. RESULTS

In the present work three cases were simulated: Reynolds number 3.200, 10.000, 25.000. The grid used in all case has 95 points in x and y direction and 65 points in spanwise direction z, The non-dimensional time step used was 0.005. A fourth order discretization was used in all cases.

The velocities profiles, the root mean square RMS) and one of the anisotropic components of the Reynolds tensor ($\overline{u^l v^l}$) are compared with experimental data of Prasad and Koseff (1989). Being

$$RMS_u = \sqrt{\overline{u^l u^l}} \tag{20}$$

and

$$RMS_v = \sqrt{\overline{v^l v^l}} \,. \tag{21}$$

The velocities profiles are compared with numerical data of Despande and Milton (1998) also. These profiles were obtained in the cavity central plane ($z = 0.5$). The velocity component u and RMS_u profile were obtained in the vertical line ($x = 0.5$), the component v and RMS_v in horizontal line ($y = 0.5$). The anisotropic components of the Reynolds tensor was obtained in both lines.

The turbulent kinetic energy spectral density k, given by:.

$$k = \frac{\langle u_i^l u_i^l \rangle}{2} \,. \tag{22}$$

of all resolved scales were obtained through eight signals samples average.

To analyze the flow topology in this work will be used, vorticity isosurface and Q criteria isosurface. It is defined as the half the difference of euclidean tensor norm at points where the vorticity tensor is larger than the deformation tensor by Jeong and Hussain (1995). An important observation is that this difference this difference decreases with the increase of the deformation norm, this occurs at the center of the eddy structures. According the definition, the equation of the criterion Q is given by:

$$Q = \frac{1}{2}\left(|\Omega|^2 - |S|^2\right) > 0 \,, \tag{23}$$

where Ω is the vorticity tensor and S is the deformation tensor.

4.1. Coomparison with literature data

In the Fig. 1 the u and v profiles are compared with the experimental results of Prasad and Koseff (1989) and the numerical results of Despande and Milton (1998) for Reynolds number 3,200 (left) and 10,000 (right). There is a good agreement between the results shown, with a slight overestimate the speed at the minimum speed of the component of u velocity profile for first case. This shows that the grid is insufficient for a direct simulation even for the lowest Reynolds number. Therefore it is necessary to model the turbulence, even for this case. The agreement is better for the other case, possibly due to the use of the Germano's dynamic model.

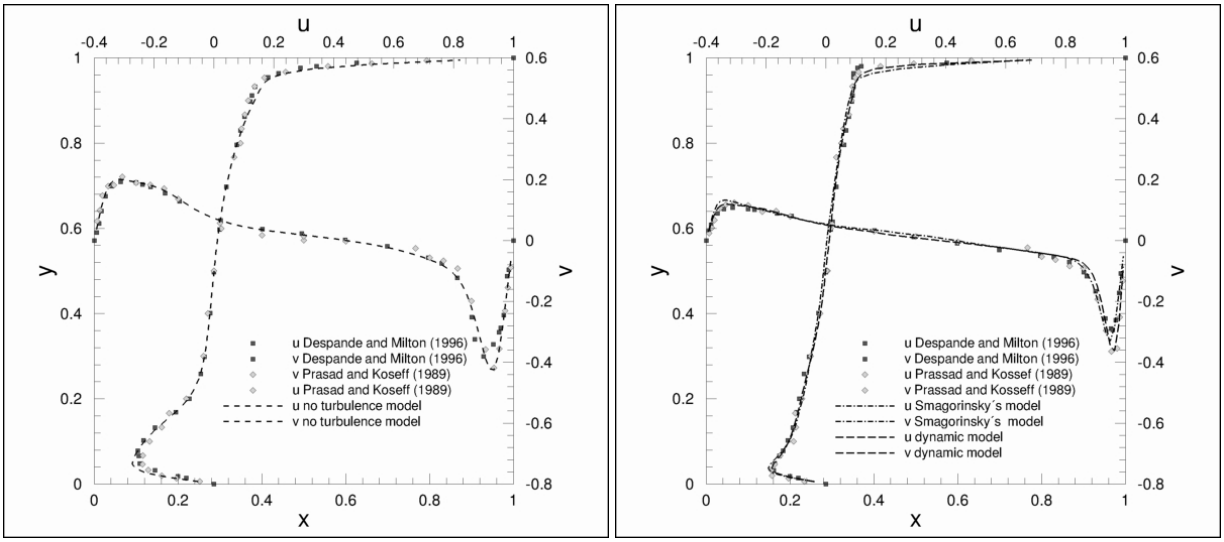

Figure 1. Velocity profiles in center lines of middle plane for Reynolds number 3200 (left) and 10000 (right).

The results obtained with this model show a difference of 0.8% for u minimum velocity value near cavity button, 5% for v maximum velocity value near the back wall and 0.4% for minimum near front wall. Note that the flow near the back wall is more complex, so large errors are expected. Tables 1 shows detailed values values for comparison for Reynolds number 3,200 and 10,000 respectively.

Table 1: Results for maximum and minimum velocities for Reynolds number 3,200 and 10,000 flow.

Result	u_{min} near button wall		v_{max} near back wall		v_{max} near front wall	
	y	u_{min}	x	v_{max}	x	v_{max}
Re = 3,200						
Prasad and Koseff (1989)	0.07816	- 0.25397	0.06334	0.19214	0.92894	- 0.38118
Despande and Milton (1998)	0.04667	- 0.23863	0.06667	0.20903	0.95333	- 0.41814
No model	0.04737	- 0.27339	0.05790	0.20061	0.95263	- 0.42439
Re = 10,000						
Prasad and Koseff (1989)	0.03206	- 0.17460	0.06334	0.10824	0.96929	- 0.28412
Despande and Milton (1998)	0.03333	- 0.18299	0.66667	0.12491	0.96667	- 0.36377
Smagorinsky's model	0.03684	- 0.19322	0.04737	0.13105	0.963158	- 0.33017
Germano's Dynamic model	0.03684	- 0.18153	0.04737	0.11856	0.973684	- 0.36235

In the Fig. 2 the RMS_u, RMS_v and $\overline{u'v'}$ profiles are compared with the experimental results of Prasad and Koseff (1989) for Reynolds number 3,200 (left) and 10,000 (right). There is a good agreement between the results shown. Observe that the shape of the profile is captured by the data, however, the peak fluctuation is not achieved, especially in the more turbulent region as in proximity of the walls.

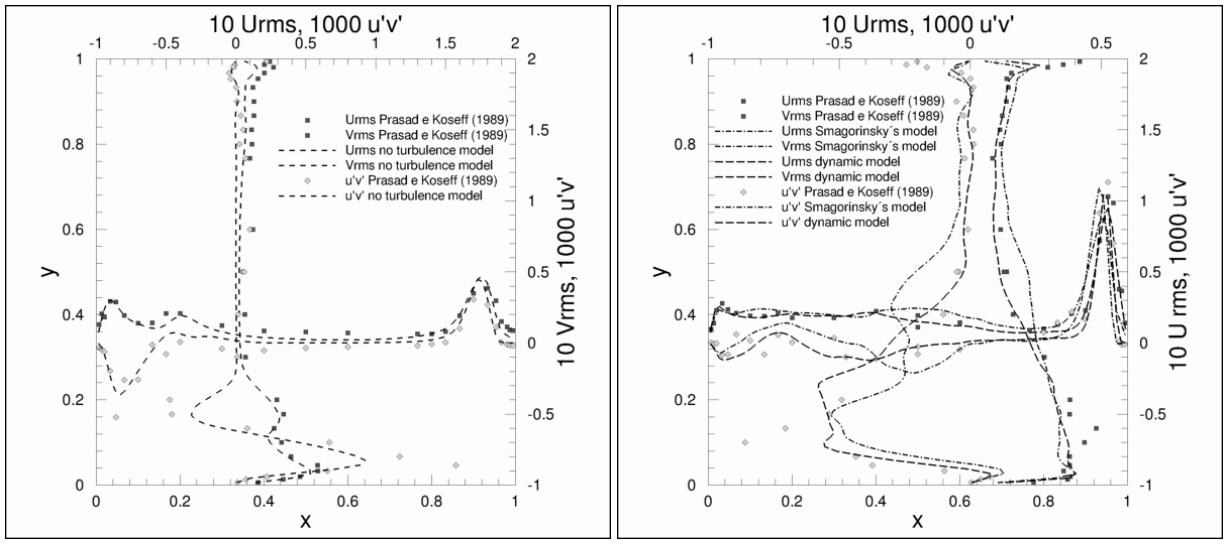

Figure 2. *RMS* and $\overline{u'v'}$ in center lines of middle plane for Reynolds number 3200 (left) and 10000 (right).

4.2. Spectral density of turbulent kinetic energy

Figure 3 (left) shows the spectral density of turbulent kinetic energy in the center, near back wall ($x=0.3$ and $y=$ ۰.۳) of the cavity obtained with dynamic modeling for Reynolds numbers 10,000. Three positions are shown. Observe that the central region ($z=0.5$) has a higher level of turbulent kinetic energy. However there is a reversal near the wall ($z=0.1$), the level of kinetic energy is greater than in ($z=0.3$). This shift can be explained by the presence of the corner vortex, since it is a toroidal structure that extends in the anterior wall near the side walls.

Figure 3 (right) shows the spectral density of turbulent kinetic energy in the center, near back wall ($x=0.3$ and $y=0.3$) of the cavity obtained with dynamic modeling for Reynolds numbers 10,000 and 25,000. We can see that for Reynolds number equal to 10,000 the level of turbulent kinetic energy is higher in larger structures at lower and lower, which indicates the formation of large structures in this case. In cases with Reynolds with 25,000 the level of turbulent kinetic energy is greater in smaller structures.

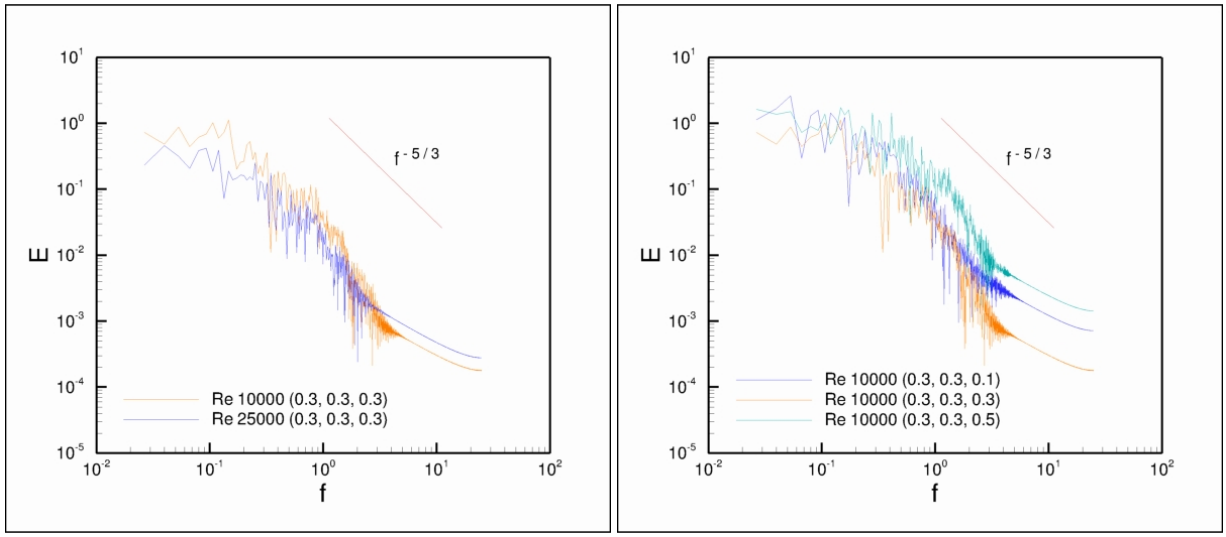

Figure 3. Turbulent energy density specters for Reynolds number 10000 (left) and in the point (0.3, 0.3, 0.3) (right).

4.3. Flow topology

The Fig. 4 (left) shows x vorticity component isosurface to the flow Reynolds number 3,200 in undimentional at time 600s. We can see three pairs of counter-rotating like Taylor-Görtler type structure. In this case, these structures have been well defined. Note the presence of the corner vortex, which is the toroidal structure near the side wall. The mean flow x vorticity component isosurface are shown in the Fig. 4 (right). In the mean flow does not persist the like Taylor-Görtler type structure, indicating that these structures are transient. However, the lateral vortices persist, which

is to be expected, since these structures is due interaction between the main flow and lateral wall, while the former are due to instabilities in the flow.

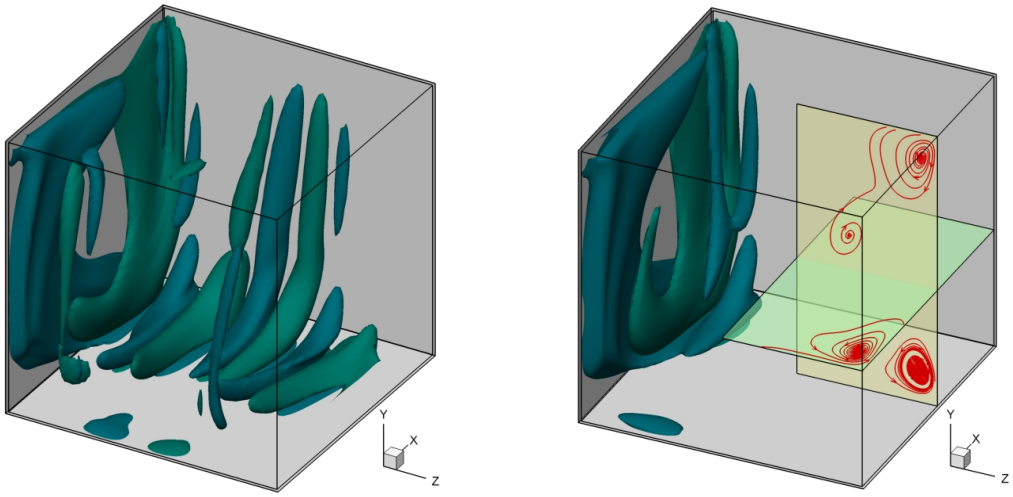

Figure 4: x direction vorticity isosurface in Reynolds number 3,200 flow at time 600s. w_x = -0,50 (blue), w_x = 0.50 (gren) (left), and for mean flow w_x = -1.00 (azul), w_x = 1.00 (verde) and streamlines in planes x = 0.58 and y = 0.42 (right) .

The flow to Reynolds number 3,200, as already noted, are considered by some authors as laminar. What can be observed with respect the topology of this flow is that the transient structures appear well defined and do not have strong deformations. But this should still be cause for much controversy. We should be noted the transition to turbulence is a problem still unresolved, even considering an apparently simple configuration as the lid driven cavity.

The transient flow for the Reynolds number of 10,000 shows like Taylor-Görtler type structure extend in the flow direction and cross toroidal structures superimposed to them. These structures can be seen in the Fig. 5 (left). This figure shows Q criterion isosurface at time 500s. These structures deform the main vortex streamlines. These structures were not found in the simulation for Reynolds number 3,200. This deformation results in a mass transfer to upper flow making uniform the u velocity profile.

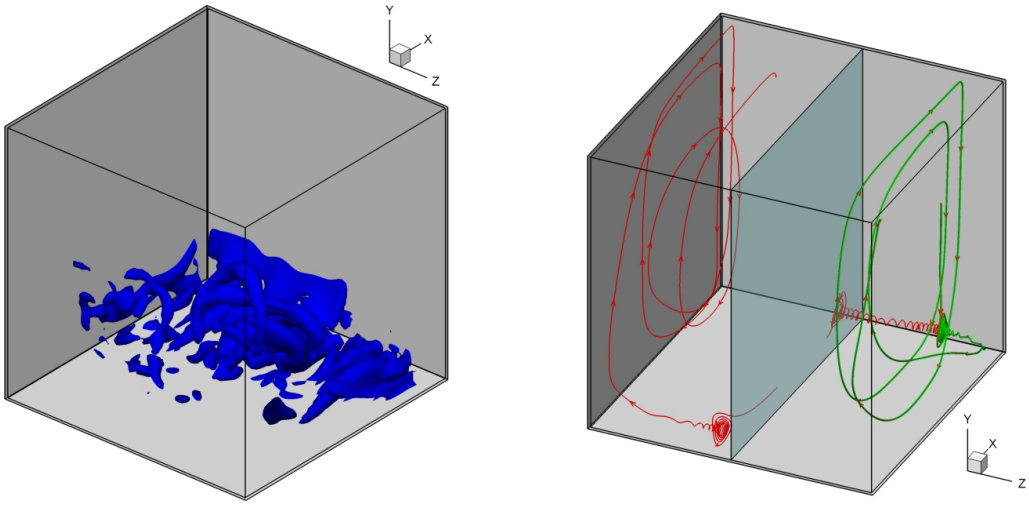

Figure 5: Q criteria isosurface equal to 2.50 in Reynolds number flow 10.000 at time 500s (left) and streamlines from secondary vortices in Reynolds number 10.000 mean flow (right).

Figure 5 (right) shows secondary vortices streamlines. There is a movement with helical turns closer in both the back and the front vortex. The front vortex presents a bifurcated structure, with the division around $z = 0.78$. The flow takes two opposite directions, one towards the plane of symmetry and the other towards the side walls. This bifurcation

appears to have a previous relationship with the remaining like Taylor-Görtler type structure in mean flow for Reynolds number 10,000.

In the flow for Reynolds number 10,000 the structures have well defined in transient flow. However they have quite deformed, which can be seen as a strong influence of small fluctuations in the structure of the flow. This fact combined with the emergence of structures in all directions at random characterized it as a fully turbulent flow. In the mean flow presents more complex structures than the flow Reynolds number 3200, in particular the bifurcation of the front secondary vortex and like Taylor-Görtler type structure.

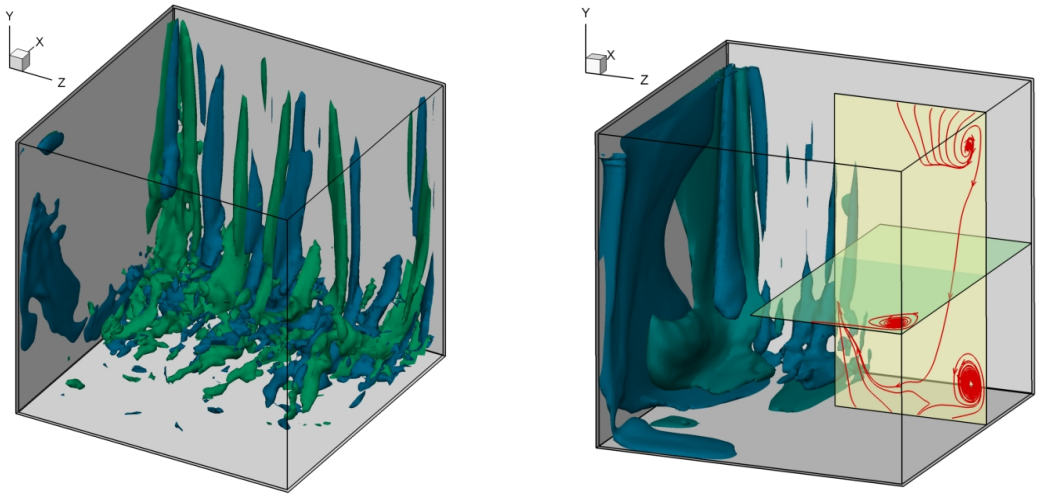

Figure 6: Isosuperfícies de vorticidade na direção *x* do escoamento a número de Reynolds igual a 25.000 no tempo igual a 400s. w_x = -2,25 (azul), w_x = 2,25 (verde)(left) (right) .

The flow to Reynolds number 25,000 has five pairs of counter-rotating like Taylor-Görtler type vortices well defined, though quite deformed. They can be seen in Fig. 6 (left). It show *x* direction vorticity isosurface at time 500s. These deformations appear to strongly influence the lateral vortices, one sees they are quite uncertain. This flow does not present cross flow coherent structures as the Reynolds number equal to 10,000. The structures are already present undefined and completely random.

For Reynolds number 25,000 the location of the front vortex bifurcation was found approximately $z = 0.77$, closest to the center than in the flow Reynolds number equal to 10,000. However you cannot come to a definite conclusion on this bifurcation, because greater Reynolds number studies are required, both to detect its occurrence and to verify its dependence on this parameter. However its influence on the flow is clear.

5. CONCLUSION

For the cases of Reynolds numbers 3,200 and 10,000 the mean velocities profiles agree well with experimental data and numerical data in the literature. The structures of the flow at Reynolds number 3200 are expected and found in the literature for this case. However, the flow Reynolds number equal to 10,000 was not presented in the literature: cross-flow coherent structures and front secondary vortex bifurcation. The flow to Reynolds number equal to 25,000 shows no strong topological changes with respect to the flow Reynolds number equal to 10,000, especially with the mean flow. But the structures in this case are more random and undefined.

6. ACKNOWLEDGEMENTS

We thanks to the Universidade Federal de Uberlândia and the Faculdade de Engenharia Mecânica for the opportunity to undertake this work and Capes and CNPq by the resources available for the completion of this work.

7. REFERENCES

Aidun, C. K., Triantafillopoulos, N. G. and Benson, J. D., 1991, “Global Stability of a Lid-Driven Cavity with Throughflow: Flow Visualization Studies”, Phisics and Fluids A, Vol. 3, pp. 2081-2091.

Boussinesq, J., 1877, “Essai sur la Théorie des Aux Courrantes”, Memorial Présente Academie de Science.

Bradshaw, P. Feb. 1997, Understanding and Prediction of Turbulent Flow – 1996, International of Heat and Fluid Flow, Vol. 18, pp. 45-54.

Burggraf, O. R., Jan. 1966, "Analitical and Numerical Studies of the Structure of Steady Separated Flol", Journal of Fluid Mechanics, Vol. 24, n. 1, pp. 113 – 151, jan.

Chiang, T. P. and Sheu, W. H., 1997, "Numerical Prediction of Eddy Structure in a Shear-Driven Cavity", Computational Mechanics, Vol. 20 pp. 379-396,.

Dean, W. R. and Montagon, P. E., 1949, "The Steady Motion of Viscous Liquid in a Corner", Proceediings Cambridge Philosophical Society, Vol.45, pp. 345.

Despande M. D. and Milton, S. G., 1998, "Kolmogorov Scale in a Driven Cavity Flow", Fluid Dynamics Researc, Vol. 22, pp. 359-381.

Ferziger, J. H. and Peric, M., 1999, "Computational Methods for Fluid Dynamics", Spriger, 2ª. edição revisada.

Freitas, C. J., Street, R. L., Findkakis, A. N. and Koseff, J. R., 1985, "Numerical Simulation of Three-Dimensional Flow in a Cavity", International Journal for Numerical Methods in Fluids, Vol. 5, pp. 561-575.

Germano, M., Piomelli, H., Moin, P. and Cabot, W. H., Jul. 1991, "A Dynamic Subgrid-Scale Eddy Viscosity Model", Phisics and Fluids A, Vol. 3, no. 7, pp. 1760-1765.

Hassan, Y. A. and Barsamian, H. R., 2001, "New-Wall Modeling for Complex Flow Using the Large Eddy Simulation Technique in Curvilinear Coordenates", International Journal of Heat and Mass Transfer, Vol. 44, pp. 4009-4026, 2001.

Jeong, J. and Hussain, F., 1995, "On the Identification of a Vortex", Journal of Fluid Mechanics, Vol. 285, pp. 69-94,.

Koseff, J. R. and Street, R. L., "Visualization of a Shear Driven of Three-Dimensional Recirculating Flow", *Jounal of Fluid Engineering*, Vol. 106, pp. 21-29, 1984.

Kolmogorov, A. N., "Equation of Turbulent Motion of an Incompressible Fluid", 1942, Izvestia Akademii Nauk, Vol. 6, pp. 56-56.

Lesieur, M. Metais, O. and Compte, P., 2005, "Large Eddy-Simulation of Turbulence", Cambridge University Press.

Lilly, D. K., "A Proposed Modification of the Germano Subgrid-Scale Closure Method", Jul. 1992, Phisics and Fluids A, Vol. 4, no. 3, pp. 633-635.

Migeon C. , Pineau, G. and Texier, A., 2003, "Three-dimensionality Development Inside Standard Parallelepipedic Lid-Driven Cavities at Re = 1000", Jounal of Fluids and Structure, Vol. 17, pp. 717-738.

Moffat, H. K., jan. 1964, "Viscous and Resistive Eddies Near a Sharp Corner", Journal of Fluid Mechanics, Vol. 18, n. 1, pp. 1 – 18.

Padilla E. L, 2004,. "Simulação de Grandes Escalas da Transição a Turbulência em Sistemas de Rotativos de Transferência de Calor", Tese de Doutorado da Universidade Federal de Uberlândia.

Pan, F. and Acrivos, A., Jun. 1967, "Steady Flow in Rectangular Cavities", Journal of Fluid Mechanics, Vol. 28, n. 4, pp. 643 – 655.

Peng, Y.-F., Shiau, Y.-H. and Hwang, R. R., Nov. 2003, "Transition in a 2-D Lid-Driven Cavity Flow", Computers and Fluids, Vol. 32, pp. 337–352.

Pergn, C. H.-Y. and Street R. L., 1989, "Three-Dimentional Unsteady Flow Simulation: Alternative Strategies for a Volume-Average Calculation", International Journal of Numerical Methods in Fluids, Vol. 9, pp. 341-162.

Prassad, A. K. and Koseff J. R., Feb. 1989, "Reynolds Number and End-Wall Effects on a Lid-Driver Cavity Flow", Physics and Fluid A, Vol. 1, p 208-2218.

Shankar P. N. and Deshpande, M. D., 2000, "Fluid Mechanics in the Driven Cavity", Annual Reviw of Fluid Mechanics, Vol. 32, pp. 93-136.

Sheu, T. W. H. and Tsai, S. F., 2002, "Flow Topology in a Steady Three-Dimensional Lid-Driven Cavity", Computers and Fluid, Vol. 31, pp. 911-934.

Smagorinsky, J., Mar. 1963, "General Circulation Experiments With the Primitive Equations: The Basic Experiment", Monthly Weather Review, Vol. 91, no. 3, pp. 99-164.

White, F. M., 2005, "Viscous Fluid Flow", McGraw-Hill Professional, 3ª Edição.

Zang, Y., Street, R. L. and Kossef, J. R., 1993, "A Dynamic Mixed Subgrid-Scale Model and Its Application to Turbulent Recerculating Flows", Physics and Fluids, Vol. 5, n. 12, pp. 3186-3196.

8. RESPONSIBILITY NOTICE

The authors are the only responsible for the printed material included in this paper.